powders

MDPI

Article

Fluidized Bed Co-Melt Granulation: New Insights in the Influence of Process Variables and Validation of Regime Map Theory

Jacquelina C. Lobos de Ponga [1,2], Juliana Piña [1,2] and Ivana M. Cotabarren [1,2,*]

[1] Departamento de Ingeniería Química, Universidad Nacional del Sur (UNS), Bahía Blanca 8000, Argentina; jlobos@plapiqui.edu.ar (J.C.L.d.P.); julianap@plapiqui.edu.ar (J.P.)
[2] Planta Piloto de Ingeniería Química, PLAPIQUI (UNS-CONICET), Bahía Blanca 8000, Argentina
* Correspondence: icotabarren@plapiqui.edu.ar

Abstract: The understanding of granule growth mechanisms and the effects of formulation and operating conditions over product quality and process performance in fluidized bed co-melt granulation is nowadays of great interest. In this sense, this work systematically studies the combined effects of binder content (W_{PEG}) and fluidization air flowrate (F_A) and temperature (T_A) on granules' quality and process-related variables (product mass (M_P), elutriated fines (M_f), mass stuck on walls (M_W)) by using a Box–Behnken-type design of experiments (DoE), as it is a statistical tool suggested by the Quality by Design (QbD) initiative. It was found that the granules' size and powder flowability are significantly affected by W_{PEG} (higher W_{PEG}, higher granule size and better flowability). Interestingly, T_A is the process variable that significantly affects M_P, enhancing process performance at high temperature values. Regarding F_A, it significantly affects d_{10}, promoting the formation of small particles due to breakage at high flowrates and the presence of non-elutriated powder at low flowrates. As a consequence, intermediate F_A is the optimum for obtaining higher M_P. Regarding regime map studies, most runs experienced a rapid growth regime, which is in accordance with the granules' high pore saturation. This result agrees with the observed high increment in particle size and the morphology of the final granules, allowing researchers to validate and extend existing previous maps.

Keywords: fluidized-bed granulation; co-melt; regime map; Box–Behnken; lactose; polyethylene glycol

check for updates

Citation: Lobos de Ponga, J.C.; Piña, J.; Cotabarren, I.M. Fluidized Bed Co-Melt Granulation: New Insights in the Influence of Process Variables and Validation of Regime Map Theory. *Powders* **2023**, *2*, 639–658. https://doi.org/10.3390/powders2030040

Academic Editor: Paul F. Luckham

Received: 29 March 2023
Revised: 25 July 2023
Accepted: 12 September 2023
Published: 15 September 2023

Copyright: © 2023 by the authors. Licensee MDPI, Basel, Switzerland. This article is an open access article distributed under the terms and conditions of the Creative Commons Attribution (CC BY) license (https://creativecommons.org/licenses/by/4.0/).

1. Introduction

Granulation is an important process step applied in the manufacturing of numerous pharmaceutical products because it improves material handling and flowability, allows obtaining a desired particle size, enhances product appearance, controls particle moisture content, and it improves compressibility, content uniformity and, in some cases, the dissolution rate of the materials once they are formulated into a final solid dosage form (e.g., tablets) [1–3]. Typically, three components are needed to produce granules: initial seeds or nuclei, mixing, and a binder. The seeds are always agitated to achieve a good binder distribution; therefore, granulators are often classified into mechanical (e.g., pans, drums, high shear granulators, twin-screw) or pneumatic (fluidized-bed granulators) agitated, according to the mixing principle. Fluidized-bed granulators offer some advantages with respect to other granulation systems, such as the simultaneous spraying, granulation, drying and/or cooling stages, and control, within certain limits, of the granule physical properties by the manipulation of some operating variables [4].

According to the binder nature, granulation processes are usually classified as wet, dry or melt. In melt granulation, particles are enlarged using binders that are in their solid states at room temperature, but they soften and flow at temperatures above their glass transition temperature or melting point [4]. The absence of water or other solvents makes this approach quite valuable for moisture-sensitive ingredients. It completely avoids the use of solvents

and the disadvantages associated with their recovery and final disposal, while it minimizes the energy cost related to solvent evaporation [5]. Furthermore, the binders are added to the system either as: (1) powders that melt during the granulation process (co-melt or in situ granulation) or (2) atomized molten liquids (spray-on melt granulation) [3].

In this sense, fluidized bed melt granulation (FBMG) has received wide interest in the pharmaceutical research field, being the most common application the preparation of pharmaceutical granules for tableting [6]. Although granulation processes involving the incorporation of the binder as droplets have received significantly more attention from a scientific point of view, both for wet and melt granulation, it is notable that co-melt processes are much more practical from an industrial point of view, since they avoid the spraying stage with hot-melt flows, leading to a simpler production process [7]. To our knowledge, for co-melt granulation, the Walker et al. have been the first to extensively study this process. Walker et al. [8–10] and Zhai et al. [11,12] explored the effect of granulation time, binder/seed mass ratio, binder viscosity, and size of the seeds on the granule's final size (Particle Size Distribution, PSD) and growth mechanisms on systems composed of lactose or glass ballotini as seeds and different size fractions of PEG (of different grades according to desired variation in viscosity) and Poloxamer. Additionally, Mangwandi et al. [13] investigated the effects of fluidization air velocity, fluidization air temperature, and granulation time on granule mean size, PSD, granule homogeneity, and strength with lactose as seeds and PEG 1500 as solid binder. Ansari and Stepanek [14] used co-melt FBMG to study the growth mechanisms in hollow granules produced from mannitol granulated with PEG flakes of different initial size. Kidokoro et al. [15] prepared granules of lactose and PEG of different grades to study the binder/seed mass ratio and fluidization air temperature on granule size and flow properties. Passerini et al. [16] compared the effects of high-shear and FBMG techniques on granule size, flow properties, granulation yield (fraction between 100 and 1400 μm) and other variables related to tablet dissolution and stability for lactose granulated with PEG 6000 and ibuprofen. Prado et al. [17] studied the ability of different formulations of Gelucire to generate granules of lactose and ibuprofen, which were able to be tableted, and their effect on granules' PSD, flowability, tablet drug release, and granulation yield. Pauli Bruns et al. [18] used co-melt FBMG to prepare sustained release matrix granules of theophylline, using talc as a filler and wax as a binder, exploring the effect of formulation variables and different size fractions of wax on granules' PSD, sphericity, process yield, granules porosity, crushing resistance, and drug dissolution time.

As it can be seen, there is a great interest in understanding the granule growth mechanisms and effects of process conditions over granules' quality. However, still there is a lack of knowledge about the predictability and modeling of FBMG. In this sense, the US Food and Drug Administration (FDA) Quality by Design (QbD) initiative encourages the use of statistical tools for improving the development of high-quality pharmaceuticals. One of these tools is the design of experiments (DoE), which allows a better understanding of how formulation and process variables can influence product quality by defining the design space. From the experimental results of a response surface design, a polynomial model, describing the relation between a response and considered factors, is built. Afterwards, graphical and/or statistical analysis is carried out to determine the optimal operating conditions in order to obtain the desired formulation properties [7]. In this sense, a reduced group of authors used DoE for elucidating FBMG under a more systematic approach. Masic et al. [19] studied the effect of binder/seed mass ratio, binder particle size and type of binder, fluidization air flowrate, and granulation time on granules' PSD and morphology, flow properties, and the tablet compression and drug release of a system of lactose and paracetamol granulated with PEG 2000 and Precirol ATO 5 as binders, using a 2^3 full factorial design. The same group [20,21] studied the granulation of paracetamol and lactose with Gelucire of different size fractions through a 2^3 full factorial design, Box–Behnken, and neural networks to evaluate the effect of binder/seed mass ratio, binder particle size, and granulation time on the obtained granules, tablets properties and granulation yield (fraction between 125 and 1250 μm). Mangwandi et al. [13] also performed studies with

a DoE approach (a two-level factorial design). Kukec et al. [7] granulated Carvediol and lactose with a poloxamer to study the binder/seed mass ratio, fluidization air temperature, and endpoint temperature on granules' PSD, morphology, flow properties, and drug release through a Circumscribed Central Composite Design. More recently, Korteby et al. [6] related granules' PSD, aspect ratio, porosity, and granulation yield with the binder/seed mass ratio, viscosity and size of the binder, and outlet temperature through another empirical technique as Artificial Neural Networks (ANNs).

Also, to find an optimal operation window from a more mechanistic approach, the so-called regime maps have been developed in order to predict granulation and enable process design at all scales based on dimensionless numbers. In comparison to the DoE approach, once the map has been developed, a reduced number of experiments must be carried out [5]. Each area of the regime map represents a granulation mechanism where the controlling parameters influence to different extents. However, a wide range of formulations, process conditions and granulators are necessary for the confirmation and validation of a regime map. In this sense, a turning point contribution is the one developed by Iveson and Litster to predict wet granulation regimes in drum granulators [22], which are extensively used to predict granulation also in high-shear granulators [23]. However, regarding FBMG, scarcely few contributions can be found related to regime map development. Indeed, the same regime map was used by the group of Walker in some of the previously mentioned contributions [9,24] to predict granulation mechanisms in FBMG, even if the type or granulation unit was different (i.e., fluidized bed).

Overall, all these studies have announced a significant potential of FBMG for the preparation of granules with excellent properties for compression into tablets, relating operating conditions to granules properties through different approaches ranging from empirical but systematic, like DoE, to more predictive over different scales, such as regime map development. However, even if the studied process and formulation variables are of great importance in the FBMG process, no incidence of the combined effect of binder/seed mass ratio, fluidization air flowrate, and fluidization air temperature is assayed given that they are critical for binder melting and the distribution process and, therefore, granules' final properties. Furthermore, other critical process performance variables such as the quantity of fines collected on the FB granulator filters and/or the granulated particles that are lost due to stickiness on the equipment wall were not studied. Therefore, it is the aim of this work to systematically study the combined effect of (1) binder/seed mass ratio, (2) fluidization air flow rate, and (3) fluidization air temperature on granules' PSD, morphology, flow properties, and process-related variables (product collected in the granulation chamber, fines generation, loss due to wall stickiness) through a DoE approach by a Box–Behnken design. Furthermore, the Walker's regime map, which has been developed for a small number of experiments at similar conditions [5], is tested to identify the growth regimes of new experimental data obtained at conditions that incorporate variations in the fluidization air flowrate and temperature. Thus, it is expected to validate the regime map theory and expand its predictability to co-melt granulation in fluidized beds.

2. Materials and Methods

2.1. Materials

The meltable binder used in this study was polyethylene glycol 6000 (PEG 6000) purchased from Sistemas Analiticos S.A. (Buenos Aires, Argentina). It has a melting point around 60 °C [25]. The binder was pre-conditioned by milling the commercial flakes using a laboratory hammer mill (Laboratory Mill 120, Perten, Stockholm, Sweden) equipped with a 2 mm hole-size sieve. After milling, PEG was sieved, and the fraction within 0.250–0.105 mm was saved to be used in the granulation process. Lactose monohydrate (HMS (NZ)) was purchased from Chutrau S.A.C.I.F. (DFE PHARMA, Buenos Aires, Argentina) and used as provided. Several key specifications of lactose are shown in Table 1. The lactose particle size distribution (PSD) was measured by a light-scattering analyzer (LA 950 V2, Horiba, Kyoto, Japan) giving the diameters reported in Table 1 (i.e., d_{10}, d_{50}

and d_{90}). The bulk density (ρ_B), tap density (ρ_T), Carr Index (CI), and angle of repose (AR) were determined as specified in Section 2.4.2. The solid density (ρ_s) of PEG 6000 and lactose was determined by nitrogen adsorption (NOVA 1200e, Quantachrome Instruments, Boyton Beach, FL, USA). This technique provides a density value that does not consider the volume of pores connected to the surface of the particle, thus giving a value very close to the solid density. The fraction of PEG 6000 used as a meltable binder has a ρ_s = 1.163 g/mL.

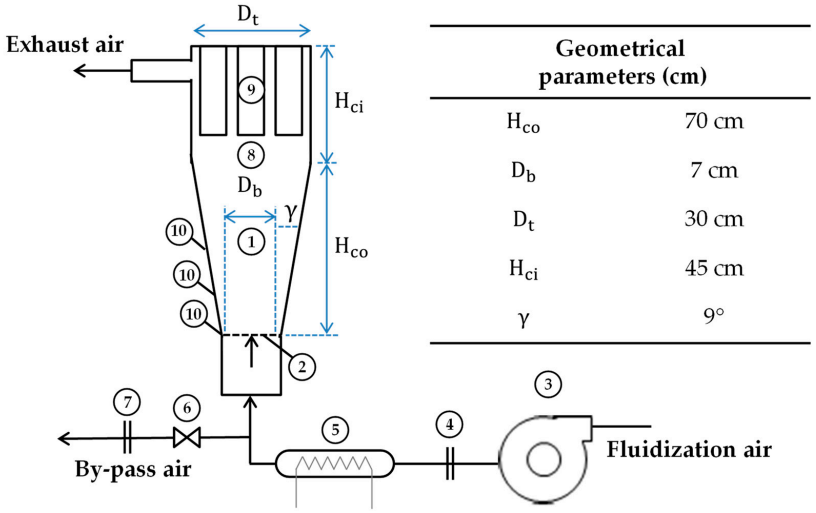
Table 1. Lactose solid properties.

Property	Value
d_{10} (mm)	0.0093
d_{50} (mm)	0.038
d_{90} (mm)	0.096
ρ_s (g/mL)	1.512
ρ_B (g/mL)	0.517
ρ_T (g/mL)	0.805
IC (%)	35.71
AR (°)	35.40

2.2. Granulation

2.2.1. Equipment

The experiments were performed in a fluidized bed granulator of ad hoc design (CONICET, Bahía Blanca, Argentina). A schematic diagram together with the chambers' geometrical parameters is shown in Figure 1. The equipment comprises a stainless-steel bottom conical vessel (1) and a cylindrical column (8) on top of it. The air distributor is a stainless-steel perforated plate (2). The fluidization air was supplied by a centrifugal blower (3) with a bypass system that can be actioned by means of a manual butterfly valve (6). This bypass allows better control of the air flow within the chamber. Before the bypass, the total fluidization air flowrate was measured by an orifice flowmeter (4) and preheated by an electrical heater (5) to maintain the air temperature at the desired level. The bypass system also presents an orifice flowmeter (7); therefore, the air flow entering the granulation chamber is inferred as the difference between the flow measured by (4) and (7) flowmeters. The elutriated fine particles were collected by a set of three filter bags located at the top of the fluidized bed freeboard (9). These filters were periodically blown back by air pulses to disengage the particulate matter. To monitor granulation temperature, the chamber was equipped with 3 thermocouples located at different distances from the air distributor (10). A Programmable Logic Control system (PLC) was used to register and control the process temperatures.



Geometrical parameters (cm)	
H_{co}	70 cm
D_b	7 cm
D_t	30 cm
H_{ci}	45 cm
γ	9°

Figure 1. Schematic representation of the experimental set-up.

2.2.2. Experimental Procedure

For each run, the granulator chamber was loaded with 150 g of solid lactose monohydrate and PEG 6000 in different mass proportions (W_{PEG}) according to the experience. The solid mixtures were previously heated to 50 °C in an oven to avoid a drop in temperature once charged to the unit. Furthermore, the granulator chamber was also previously heated by means of the fluidization air at the desired process temperature (T_A). Once the solids were charged in the unit, fluidization air was again turned on at a set flowrate (F_A), which was determined by the aperture of the bypass valve (V_A). A controller manipulates the fluidization air inlet temperature (T_A) to maintain the temperature at the specified value. Once the thermal regime of the bed was established, the granulation was carried out for 20 min. After that, the fluidization air temperature was turned down, allowing the granules to cool. Once the granules' temperature reached 30 °C, the fluidization air was turned off, and the run stopped. Afterwards, the material deposited in the different parts of the granulation unit—granulation chamber (M_P), walls (M_W), and filters (M_f)—were collected and separately saved in hermetically sealed plastic bags for characterization. The granules collected in the granulation chamber (M_P) were considered as each run product.

2.3. Experimental Design

To evaluate the influence of the main operating parameters on the properties of the obtained granules and process conditions, we used a Box–Behnken incomplete factorial design consisting of three factors with three central points: % aperture of bypass valve (X_1), binder mass content (X_2), and fluidization air temperature (X_3). These were selected according to similar works in which these variables had significant effects, and the settings were determined based on the equipment practical considerations and the authors' initial experimentation and prior experience. Since Box–Behnken designs are specially made to require only three levels, coded as −1, 0, and +1, the factor levels chosen in terms of actual values were X_1 = 0, 50, 100%; X_2 = 10, 15, 20 wt%; and X_3 = 80, 90, 100 °C. In the case of X_1, the variable that is manipulated at the end is the fluidization air flowrate that, as explained in Section 2.2.1, is determined by the difference between the total fluidization air flowrate and the one derived to the bypass according to the valve % aperture setting; the higher the aperture, the lower the fluidization air flowrate for the granulation chamber.

As responses, several variables were studied. Regarding the produced granules, the following variables were analyzed: size distribution (by estimation of representative granule diameters d_{10}, d_{50}, d_{90}), angle of repose (AR), mass of granular product collected in the chamber (M_P), mass of fines (M_f), and mass on the walls (M_W).

A matrix design was performed using the Design Expert 10.0 software (Trial version, Stat-Ease, Inc., Minneapolis, MN, USA), which consisted of 15 runs with the combination of factors and levels shown in Table 2. The software was used to find suitable fitting models in which the coefficients were calculated based on the experimental responses. Multiple quadratic regression models were obtained from the full or reduced following equation:

$$\hat{y} = \beta_0 + \sum_{i=1}^{4} \beta_i x_i + \sum_{i=1}^{3} \beta_{ii} x_i^2 + \sum_{i=1}^{3} \sum_{j=i+1}^{4} \beta_{ij} x_i x_j \quad (1)$$

where $\hat{y}$ is the response studied, β_0 is the intercept, β_i is the main effect coefficient for the ith factor, β_{ii} is the quadratic effect coefficient for the ith factor, β_{ij} is the model coefficient for the interaction between factors ith and jth, and x_i and x_j are each of the considered factors. ANOVA was used to determine the statistical significance of the model factors. Model terms with p-values less than 0.05 were considered significant, and non-significant terms were deleted from the equation except when they increased the quality of the fit. The adequacy of the developed regression models was evaluated by calculation of the modeling statistical coefficient R-squared (R^2) and the adequate precision (AP) which is a measure of the signal-to-noise ratio. An AP value greater than 4 is desirable to use the model to navigate the design space. Last but not least, the lack of fit value (LOF) should

not be significant (i.e., LOF p-values should be higher than 0.05 to indicate that the model fits the data well) [26].

Table 2. Experimental design matrix used to evaluate the granulation process with factors as actual values and corresponding responses.

Run	X_1 (%)	X_2 (wt%)	X_3 (°C)	d_{10} (mm)	d_{50} (mm)	d_{90} (mm)	AR (°)	M_P (g)	M_F (g)	M_W (g)
G1	0	10	90	0.03	0.31	0.72	20.6	109	11	11
G2	100	10	90	0.02	0.22	0.74	33.4	134	4	3
G3	0	20	90	0.07	0.71	0.97	13.9	128	11	6
G4	100	20	90	0.24	0.72	1.45	13.1	137	8	0
G5	0	15	80	0.03	0.75	1.50	18.4	110	24	6
G6	100	15	80	0.02	0.07	0.19	20.3	93	39	6
G7	0	15	100	0.20	0.29	0.71	18.3	125	5	2
G8	100	15	100	0.21	0.28	0.55	16.4	136	3	5
G9	50	10	80	0.09	0.72	1.08	10.4	122	12	11
G10	50	20	80	0.12	1.63	1.83	9.2	100	35	8
G11	50	15	100	0.13	0.32	0.73	15.6	130	7	5
G12	50	20	100	0.23	0.35	1.14	14.5	135	2	1
G13	50	15	90	0.22	0.31	0.42	19.9	130	7	4
G14	50	15	90	0.22	0.31	0.48	18.9	135	5	1
G15	50	15	90	0.26	0.51	0.79	15.2	137	4	4

2.4. Characterization of the Granules

2.4.1. Particle Size Distribution

The PSD of the product granules was evaluated by sieving analysis using a vibratory sieve shaker (ZONYTEST EJR 2000, Zonytest, Argentina) and a series of standard sieves in a range from 3.36 to 0.053 mm following a $2^{1/2}$ progression. Sieve analysis was performed by duplicate, with each sample weighing 30 g and 15 min of sieving time. d_{10}, d_{50}, and d_{90} were determined from the mass cumulative distribution.

To further characterize the granules, the morphology of the external surface of some selected granules (G1, G3, and G5) was assessed in an EVO 40-XVP, LEO Scanning Electron Microscope (SEM). The samples were previously metalized with gold in a PELCO 91,000 sputter coater.

2.4.2. Bulk and Tapped Densities. Carr Index. Angle of Repose

Bulk densities (ρ_B) of granules and lactose powder were measured by pouring 1.5 g in a 10 mL graduated cylinder and calculated as the ratio between the weight of the sample and the occupied volume. The tapped density (ρ_B) of the same samples was measured by tapping the cylinder 100 times and registering the final volume.

For the same purpose, the angle of repose (AR) was determined by pouring 1.5 g of granules or lactose powder through a funnel located at a fixed height on a flat horizontal surface of fixed radius (r) and measuring the height (h) of the conical pile formed. The tangent of the angle of repose is given by the h/r ratio [27].

Powder compressibility was evaluated using Carr's compressibility index (CI), which was estimated by Equation (2) [28]:

$$CI = \frac{\rho_T - \rho_B}{\rho_T} \times 100 \quad (2)$$

All samples were analyzed at least in triplicate.

2.4.3. Granule Porosity

To determine the granules' porosity (ε), the envelope density (ρ_E) was tested by using a pycnometer and ethanol as the displacement fluid, considering both lactose and PEG

6000 insolubility or very low solubility in this substance. Afterwards, the samples' solid density was estimated from the lactose, and the PEG 6000 solid density was determined by nitrogen adsorption according to the corresponding mass fraction for each run. Then, the porosity of granules was calculated by Equation (3).

$$\varepsilon = 1 - \frac{\rho_E}{\rho_S} \tag{3}$$

2.5. Granulation Performance

The granulation performance was evaluated in terms of the mass of the granular product collected in the chamber (M_P). The process losses were estimated by weighting the material collected in the filters (M_f) and on the chamber walls (M_w).

2.6. Regime Map

To elaborate Walker's regime map, it is necessary to estimate for the system the Stokes deformation number (St_{def}) and the maximum pore saturation (s_{max}) given by the dimensionless groups presented in the following equations:

$$St_{def} = \frac{\rho_g U^2}{2Y_g} \tag{4}$$

$$s_{max} = \frac{w\rho_{SS}(1-\varepsilon)}{\rho_L \varepsilon} \tag{5}$$

where ρ_g is the granules' density, U the inter-granule collision velocity, Y_g is the granule dynamic yield stress, w is the mass ratio of liquid to solid, ρ_{SS} is the solid seeds density, ρ_L is the liquid binder density, and ε is the granules' porosity.

For s_{max}, w was determined from the binder/solid ratio for each run, ρ_{SS} and ρ_L were the ones measured by nitrogen adsorption, and ε represents the granules' porosity estimated as explained in Section 2.4.3. Regarding the Stokes deformation number, ρ_g was estimated as ρ_E (Section 2.4.3), and the granule collision velocity for simplicity was approximated as the superficial gas velocity, while Y_g was more challenging to determine. According to Walker et al. [9], the granule dynamic yield stress should be replaced by the characteristic flow stress of the particle–binder slurry τ_g, whose results, of course, are quite complex to determine. The same authors proposed, in another contribution, a novel technique to measure τ_g, based on a compression test at temperatures similar to the ones experimented by the granules during the granulation process [10]. Based on this, an ad hoc procedure was implemented in this contribution that consisted of measuring granules' compression breakage strength using a Texture Analyzer (TA Plus Lloyd Instruments, England) equipped with a 50 N cylindrical load cell. The deformation behavior and fracture strength of individual granules corresponding to the selected representative runs (G1, G3, G5 and G8) were measured by compression between a stainless-steel base and a cylindrical probe of 5 mm diameter. The probe descended at a constant velocity of 1 cm/min. The test was carried out at least for 10 granules from each run, which were manually selected from the fraction retained between 1.19 and 1.68 mm sieves. The granules were heated on a hotplate, for at least 5 min prior to compression testing, to a temperature equal to the average chamber temperature (T_{TEST}) of the corresponding test. In this way, the first appreciable fall of the force–deformation curve was considered as the granule breakage point. The particle–binder slurry flow stress, τ_g, was taken to be proportional to the breakage force divided by the cross-sectional area of the granules. Image analysis of the granules selected for the compression test was carried out to determine each particle's cross-sectional area.

3. Results and Discussion

3.1. Experimental Design

3.1.1. Characterization of the Granules: Particle Size Distribution and Flow Properties

Table 2 presents the combination of factors and levels for the 15 runs together with the corresponding experimental results obtained for responses d_{10}, d_{50}, d_{90}, and AR. Also, the responses M_P, M_f, and M_w are shown, which will be discussed in Section 3.1.2. Furthermore, Table 3 presents the analysis of variance (ANOVA) for the same responses, which were analyzed by the application of response surface methodology. The *p*-values for each model term of the fitted responses, as well as the corresponding statistical coefficients, are presented. The corresponding regression equations are presented in the Appendix A. As shown, the binder mass content results showed significant factors for all the analyzed responses. The fluidization air temperature significantly affects d_{10} and d_{50}, while the air flowrate (% aperture of bypass valve) only presents a significant term for d_{10}. It is also important to note that the statistical coefficients values were reasonable for all responses, with R^2 greater than 0.75 for all cases, except AR (R^2 = 0.62). Furthermore, the AP is higher than 4 in all cases, indicating a good signal-to-noise ratio, and the LOF is not significant.

Table 3. Statistical values and coefficients of the mathematical models in terms of coded factors for d_{10}, d_{50}, d_{90} and AR response variables.

Source [a]	d_{10} (mm) R^2 (0.88)		d_{50} (mm) R^2 (0.81)		d_{90} (mm) R^2 (0.75)		AR R^2 (0.62)	
	Coeff.	***p*-Value**	**Coeff**	***p*-Value**	**Coeff**	***p*-Value**	**Coeff**	***p*-Value**
β_0 [b]	0.23		0.45		0.55		16.87	
X_1	0.02	0.2342	−0.0962	0.2825	−0.1212	0.2796		-
X_2	0.0487	**0.0156**	0.23	**0.0272**	0.265	**0.0350**	−3.660	**0.0317**
X_3	0.0637	**0.0043**	−0.2412	**0.0224**	−0.1837	0.1169	-	-
X_1X_2	0.045	0.0771	-	-	-	-	−3.394	0.1328
X_1X_3	-	-	0.1675	0.1951	0.2875	0.0878	-	-
X_2X_3	-	-	−0.22	0.1019	-	-	-	-
X_1^2	−0.0854	**0.0069**	−0.1561	0.2390	-	-	4.231	0.0777
X_2^2	−0.0579	**0.0375**	0.2513	0.0771	0.4340	**0.0222**	-	-
X_3^2	−0.0329	0.1888	-	-	0.2015	0.2254	−3.599	0.1254
AP		7.524		8.263		6.102		7.742
LOF		0.1897		0.1651		0.3015		0.2559
Model *p*		**0.0076**		**0.0383**		**0.0381**		**0.0339**

a: X_1, aperture of bypass valve; X_2, binder mass content; X_3, fluidization air temperature. b: intercept term. R^2, R-squared; AP, adequate precision; LOF, lack of fit. Statistical significance of the model terms: significant $p \leq 0.05$; non-significant, *p* greater than 0.05.

As it can be seen in Figure 2a, d_{10} increases as W_{PEG} increases. The same trend regarding binder mass content was observed by several authors that studied FBMG with or without DoE [7–9,19]. Regarding air temperature, it significantly affects the fines in the collected product; as it can be seen in Figure 2a, the higher the temperature, the higher the d_{10} value, indicating that a decrease in binder viscosity favors the particle growth of small granules. A similar effect was observed by Walker et al. [8], who found bigger granules for lower viscosity binders. Interestingly, the quadratic term of fluidization air flowrate inversely significantly affects d_{10}; this would mean that as the fluidization air flowrate increases (0% aperture of bypass valve), particles with a smaller size are retained in the granulator product, which can be observed in Figure 2b (for W_{PEG} and T_A at intermediate levels). However, d_{10} also tends to decrease for the lowest fluidization air flowrate (100% aperture of bypass valve). This indicates that at low air velocities, more fines are retained in the product, which is reasonable since they cannot be elutriated. As the air velocity increases, d_{10} starts to increase, having its maximum at intermediate air flowrates. High air velocities tend to decrease d_{10} again, which is probably due to the breakage or damage suffered by the formed agglomerates during the process, which experiences more intense

impacts. Fluidization air velocity has been previously studied only by Masic et al. [19] and Mangwandi et al. [13]. Masic et al. [19] found that fluidization air velocity alone (i.e., not in combination with air temperature) is not a significant factor for their system. On the other hand, Mangwandi et al. [13] found that air velocity strongly affects drug content and granule strength when studied in combination with air temperature.

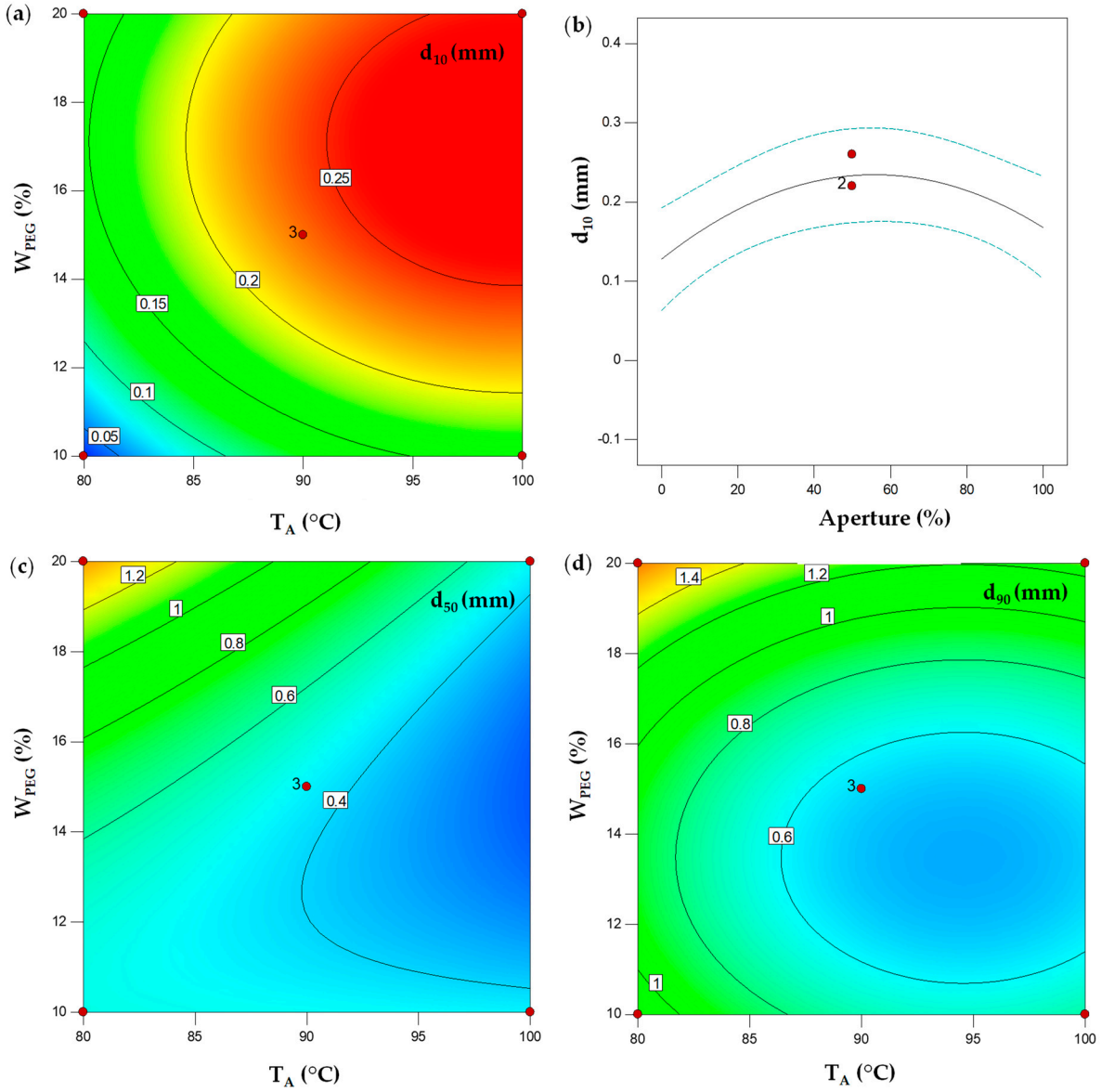


Figure 2. Contour plots for variations in binder mass content (W_{PEG}) and fluidization air temperature (T_A) for d_{10} (**a**), d_{50} (**c**), and d_{90} (**d**) at 50% bypass valve apertures. d_{10} for variations in bypass valve apertures (**b**) with other factors at intermediate level.

Regarding d_{50}, Figure 2c shows an increasing trend with W_{PEG}. As expected, the more binder in the system, the more the particles grow. Air temperature is the other significant factor for this variable; however, the tendency is the opposite to the one observed for d_{10}. In fact, according to the corresponding model coefficients (Table 3), d_{10} presents a coefficient for $X_3 = 0.0637$ (positive), while for d_{50}, it is $X_3 = -0.2412$ (negative), indicating a direct relation for the first and an inverse one for the second. As shown in Figure 2c, bigger granules are obtained for lower air temperature. Indeed, temperature affects binder viscosity, which, in turn, influences the balance between the inertial forces (generated by the collisions between particles) and the cohesive forces (viscous forces of the formed liquid

bonds between particles). The observed behavior suggests that at low temperatures, the binder's higher viscosity favors the dominance of viscous forces that tend to keep the particles stuck together, independently of its size. At higher temperatures, the size of the intermediate particles generates inertial forces higher than the viscous ones; therefore, the bonds are not resistant enough, and the granules tend to separate, decreasing d_{50}. For small particles, viscous forces are always higher than inertial ones, independently of binder viscosity variation with temperature, which favors that d_{10} always increases with temperature. This effect was also proposed by Mangwandi et al. [13], who stated that it is logical to expect a high rate of granule breakage at higher temperatures, since decreasing the binder viscosity reduces the strength.

For d_{90}, the only variable that significantly affects the response is binder mass content. As it can be seen in Figure 2d, higher binder contents favor bigger granules (i.e., higher d_{90}), although d_{90} tends to increase, in a lesser extent, for lower binder mass contents, as its quadratic term is significant as well.

The flow properties of powders can be described according to the obtained repose angle values. For AR, flow between 25 and 30° is excellent, among 31–35° the flow is good, within the range 36–40° the flow is fair, and for values higher than 41°, the powder has bad flow properties [29]. As shown in Table 2, AR values are smaller than 30° for all runs, which means excellent flow, except for one experience where this value falls within good flow. Regarding the statistical analysis for this response, Table 3 shows that AR is significantly affected only by binder mass content. As W_{PEG} increases, the angle of repose decreases, becoming a better flowing material. In fact, this model presents a coefficient for $X_2 = -3.660$, indicating an inverse response with respect to the factor; that is, the higher the binder mass content, the lower the angle of repose. Indeed, it is well known that bigger particles favor powders flow. As previously seen, a higher binder mass content increases the granules size (higher d_{10}, d_{50}, and d_{90}), giving as a result smaller AR values. To complement this result, Figure 3 presents the measured CI for all runs. Carr´s compressibility scale is more specific than AR, indicating excellent flow for values of 10%, good flowability between 11% and 15%, fair flow between 16% and 20%, acceptable flow between 21% and 25%, and poor flow between 26% and 31% [29]. As it can be seen, the granules produced in 11 out of the 15 runs have excellent flow, while 1 run gives a product with good flow, 2 runs give a product with fair flow, and only 1 run gives a product with poor flow. Again, it is possible to observe that a higher binder mass content improves flowability (lower CI), while no specific trend with fluidization air flowrate (% aperture of bypass valve) or air temperature is seen. Both Masic et al. [19] and Kukec et al. [7] reported similar findings, demonstrating that a higher binder content led to better flowability of the granules due to bigger particles and narrower particle size distributions obtained under those conditions.

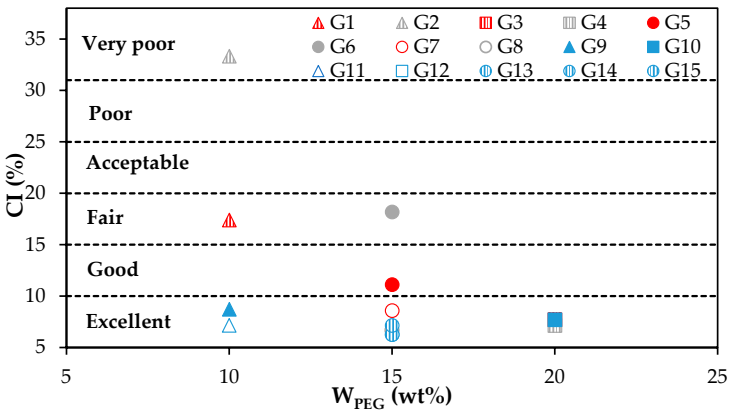


Figure 3. CI values for all runs. Symbols for W_{PEG}: square: 20 wt%, circle: 15 wt%, triangle: 10 wt%. Colors for bypass valve aperture: red: 0%, blue: 50%, gray: 100%. Infill for T_A: solid: 80 °C, striped: 90 °C, empty: 100 °C.

Powders flow is also enhanced by particles that present high sphericity and smooth surfaces. To illustrate the difference in granules surface as the amount of binder is modified, SEM images of two selected runs, G1 and G3, are shown in Figure 4. Both runs present the same settings for aperture of bypass valve and fluidization air temperature, but they also have minimum and maximum values of binder mass content. Figure 4a,b correspond to two magnifications of a representative granule of run G1, which was obtained with 10 wt% of PEG. The surface in this case is irregular, which is probably due to granules of lactose and PEG that come into contact and stay as agglomerates. Indeed, G1 presents a CI of 17.4, indicating acceptable flow. In Figure 4c,d, a surface formed by smaller particles, and overall, smoother is found. This granule corresponds to a run with a high amount of binder (20 wt%) and a product that presents a CI of 7.69, which is well within the range of excellent flow. As more binder is present, more liquid remains available in the granules surface, allowing small ungranulated lactose particles to stick to it and giving a layering growth with particles engulfment. Aleksic et al. [21] and Masic et al. [20] also found that when large binder particles (with respect to seeds, as in the present study) were used in combination with a higher binder content, larger granules with smooth surfaces (i.e., surfaces with more saturated binder) were formed. This led to excellent flow properties in the resulting granules. Similarly, Korteby et al. [6] observed that when a low binder content was used, fragile and low-density granules with a low degree of sphericity were formed.

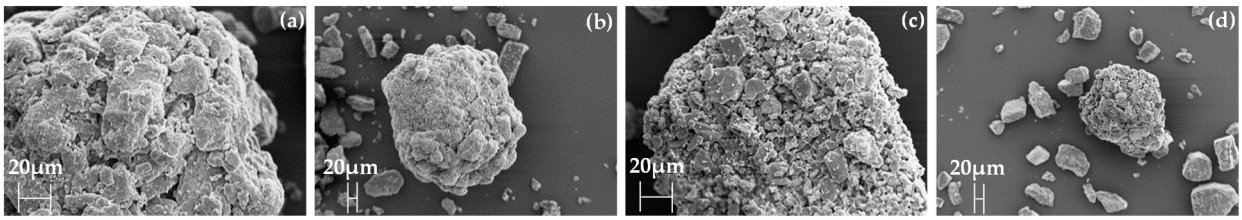


Figure 4. SEM images. (**a**) Run G1 granule x1500, (**b**) Run G1 granule x450, (**c**) Run G3 granule x1500, (**d**) Run G3 granule x450.

These results indicate that granulation, with any combination of factors, greatly improves the initial lactose powders' flowability, either by increasing particle size or giving granules with smooth surfaces. Indeed, lactose has an AR of 35.4° and CI of 35.71%, corresponding to fair and poor flow, respectively.

3.1.2. Granulation Performance

Table 4 shows the ANOVA for M_P, M_f, and M_w. The corresponding regression equations are presented in the Appendix A. As shown, the fluidization air temperature was shown to be a significant factor for all analyzed responses, while the binder mass content significantly affected the mass collected on the walls as a linear term, and in the filters, in the term interacting with air temperature. The statistical coefficients values were reasonable for all responses, with R^2 greater than 0.71 for all cases, an AP higher than 4, and a not significant LOF.

Table 4. Statistical values and coefficients of the mathematical models in terms of coded factors for M_P, M_f, and M_W response variables.

Source [a]	M_P (g) R^2 (0.85)		M_f (g) R^2 (0.93)		M_W (g) R^2 (0.71)	
	Coeff.	*p*-Value	Coeff	*p*-Value	Coeff	*p*-Value
β_0 [b]	133.45		5.15		3.23	
X_1	3.6	0.2719	0.37	0.8166	−1.29	0.1257
X_2	0.59	0.8499	2.75	0.1207	−1.89	**0.0359**
X_3	12.6	**0.0055**	−11.63	**0.0001**	−2.23	**0.0172**
X_1X_2	−4	0.3785	-	-	-	-
X_1X_3	7.06	0.1447	−4.25	0.0949	-	-

Table 4. *Cont.*

Source [a]	M_P (g) R^2 (0.85)		M_f (g) R^2 (0.93)		M_W (g) R^2 (0.71)	
	Coeff.	*p*-Value	Coeff	*p*-Value	Coeff	*p*-Value
X_2X_3	7.09	0.1433	−7	**0.0155**	-	-
X_1^2	−6.06	0.2151	3.48	0.1715	-	-
X_2^2		-		-	1.73	0.1588
X_3^2	−11.51	**0.0389**	8.98	**0.0057**	1.52	0.2081
AP		6.496		11.583		6.839
LOF		0.1203		0.0838		0.4694
Model *p*		**0.0464**		**0.0016**		**0.0288**

a: X_1, aperture of bypass valve; X_2, binder mass content; X_3, fluidization air temperature. b: intercept term. R^2, R-squared; AP, adequate precision; LOF, lack of fit. Statistical significance of the model terms: significant $p \leq 0.05$; non-significant, *p* greater than 0.05.

As shown in Figure 5a, the mass collected in the chamber increases with air temperature, which could mean that settings with low binder viscosity (i.e., high operation temperature) favor the formation of granules that remain in the chamber. This is expected since having a lower viscosity binder favors its spreading on the particles surface, which in turn allows granules' growth.

For the mass collected in the filters, again, it significantly depends on air temperature as well as its interaction with W_{PEG}. As shown in the response surface of Figure 5d, M_f increases with W_{PEG} for low temperatures, while the opposite trend, for much lower values of M_f, is observed at high temperatures, indicating an interaction between both factors. This is consistent with the findings previously observed: that at low T_A, less product is collected in the granulator chamber. Low temperatures favor a high viscosity of the binder, which hinders its spreading on the initial seeds' surface, leaving more un-granulated particles able to be elutriated. In fact, it is possible that a portion of the binder droplets remain as such and solidify without even reaching a seed particle. The more binder there is in the system, the higher the probability of having this droplet solidification, which can explain the increment of fines at low temperatures and high W_{PEG}.

Regarding the mass collected on the walls (Figure 5c), it is significantly affected by both binder mass content and fluidization air temperature. Interestingly, low W_{PEG} and low T_A favor materials' stickiness to the walls. Again, low temperatures correspond to the most unfavorable setting for M_P, since both M_W and M_f are maximum, confirming mass balance closure. This can be attributed again to the effect of binder viscosity that generates stronger bonds at high viscosities (low temperatures); therefore, if granules coated with liquid binder reach the walls, the particle–wall liquid bridges are strong enough to remain stuck.

Regarding fluidization air velocity, even if it is not a statistically significant factor for any of the three analyzed responses, it is worth studying its effect, as it helps with understanding the particle's growth mechanisms. Figure 5d–f show the variation of M_P, M_f, and M_W with the aperture of bypass valve for all the other factors on an intermediate level. As it can be seen, when the bypass valve is 0% open, which means high air velocity, M_P is minimum, indicating that either ungranulated particles are able to be elutriated or that the particles that reach the walls remain adhered to them. Indeed, high velocities favor the entrainment of particles, which corresponds to the high mass on filters observed for 0% bypass valve aperture. At the same time, high air flowrates tend to generate higher temperatures in the granulation chamber, since there is more hot mass circulating, which favors binder melting. Furthermore, particle–wall collisions are also more frequent at high air velocities. If more particles covered with melted binder reach the wall, there is more probability for them to stay adhered to the chamber, which reflects the maximum of M_P at this same setting of bypass valve aperture. On the contrary, lower fluidization air flowrates (100% bypass valve aperture) lead to lower temperatures within the chamber that can hinder granulation, leaving more ungranulated powder able to be elutriated. This

is probably the reason why M_f increases again for 100% bypass valve aperture, while M_P is minimum at this setting.

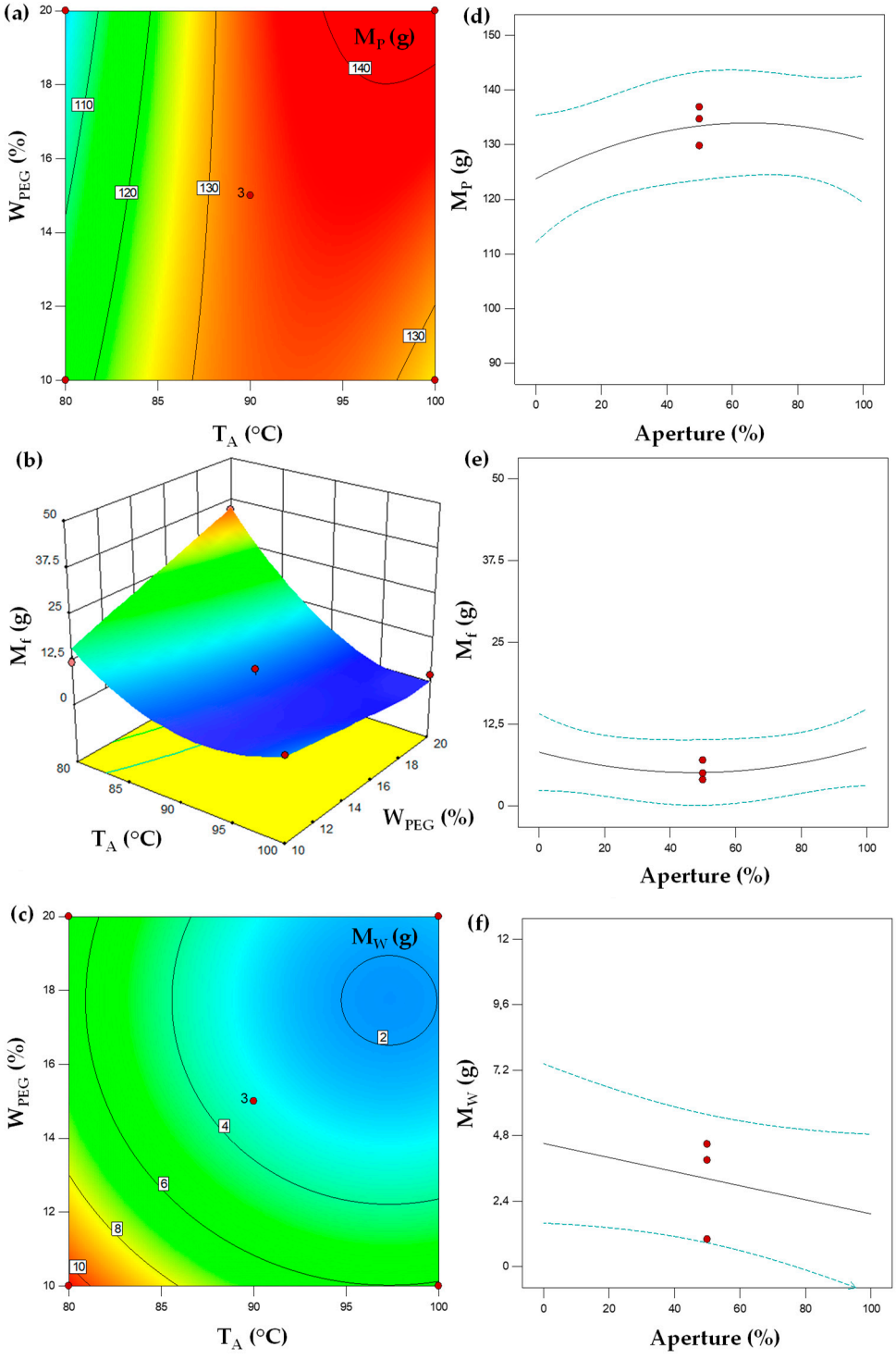


Figure 5. Contour plots and surface response for variations in binder mass content (W_{PEG}) and fluidization air temperature (T_A) for M_P (**a**), M_f (**b**), and M_W (**c**) at 50% bypass valve apertures. M_P (**d**), M_f (**e**), and M_W (**f**) for variations in bypass valve apertures with other factors at intermediate level.

Overall, the combination of variables that most favor granulation with respect to process yield and less material losses is high temperature with high binder mass content at

intermediate or low fluidization air velocities. This has not been previously reported and is an important result when defining the overall process performance.

3.2. Regime Map

As described in the Introduction section, a semi-empirical approach to understanding the granulation process has been the well-known regime map study. This approach requires deeply understanding the effect of influencing parameters, such as formulation properties, process parameters and equipment parameters to determine convenient dimensionless groups that allow localizing a particular operation regime. Once the limits between the different growth regimes have been established, it is possible to define a design space in order to keep the dimensionless parameters constant or within the same operating window across different scales [5].

Even if there exist different approaches for regimes' maps development, the one proposed by Iveson and Litster to predict wet granulation regimes in drum and high-shear granulators [22,23] is, to our knowledge, the only one that has been extended to predict granules' growth in FBMG, which was completed by Walker´s group [9,24]. In Iveson and Litster's map, the dominant granulation mechanism is characterized by calculating the St_{def} (Equation (4)), which represents the ratio of externally applied kinetic energy and the energy required for deformation, and the s_{max} (Equation (5)), that reflects the system liquid content.

In general, these growth regime studies have proposed for FBMG that, initially, granules are mainly obtained by two different nucleation mechanisms: distribution (molten binder is distributed on the surface of the solid particles) and immersion mechanisms (solid particles are immersed into the surface of the molten binder droplets). In some previous studies on FBMG [30], it was found that the prevalence of one or the other mechanism is mainly governed by the ratio between the size of molten binder particles (droplets once they melt) and the size of solid particles. Nucleation by immersion and subsequent layering with small solid particles is promoted by larger molten binder droplets, while nucleation by distribution and further growth by coalescence or agglomeration occurs when the molten binder droplets are not greater than the solid particles.

Once the nucleation phase is completed, two main types of growth can be distinguished: steady growth and induction-type growth. Steady growth occurs when granules deform and coalesce easily (high St_{def}); the collision facilitates liquid binder to squeeze out to the granules' surface, generating new areas of contact where new bonds can be formed. If these bonds are resistant enough, larger granules are formed. In this regime, the growth rate increases when more binder is present in the system (high s_{max}). In contrast, induction behavior occurs when the granules possess low deformability (low St_{def}) and is characterized by the deficient formation of contact area. Clumps of granules can break easily as the bonds are weak. The duration of the induction period decreases with increasing liquid level [5]. At high liquid contents (s_{max}~100%), rapid growth occurs since sufficient liquid arises in the surface that facilitates strong bond formations. Further liquid addition (s_{max} > 100%) causes a transition to an over-wet mass [22]. If the system is exposed to high impact velocities (very high St_{def}), no permanent granules are generated, as they are too weak to resist any separating forces, and a crumb behavior is exhibited [5].

With the aim of extending the FBMG regime map developed by Walker and coworkers, the dimensionless numbers s_{max} and St_{def} presented in Section 2.6 need to be calculated. To this end, and as it was mentioned in the Materials and Methods section, it was necessary to measure the characteristic flow stress of the particle–binder slurry (τ_g) by the compression tests at granulation temperatures described in Section 2.6. Figure 6 shows a typical stress–deformation profile obtained in these tests. The arrow indicates the value taken as the stress of the particle–binder slurry, considering that it is estimated as the force value registered during the compression tests divided by the projected area of the granule obtained by image analysis prior to the assay. Table 5 summarizes the average τ_g values and deviations for all the tests. As it can be seen, the flow stress presents variations between the different samples, although no direct relation with operating conditions can

be established. Consequently, it was decided to take for all runs an average value for τ_g of 0.045 MPa. Using this value, St_{def} values for all runs were calculated.

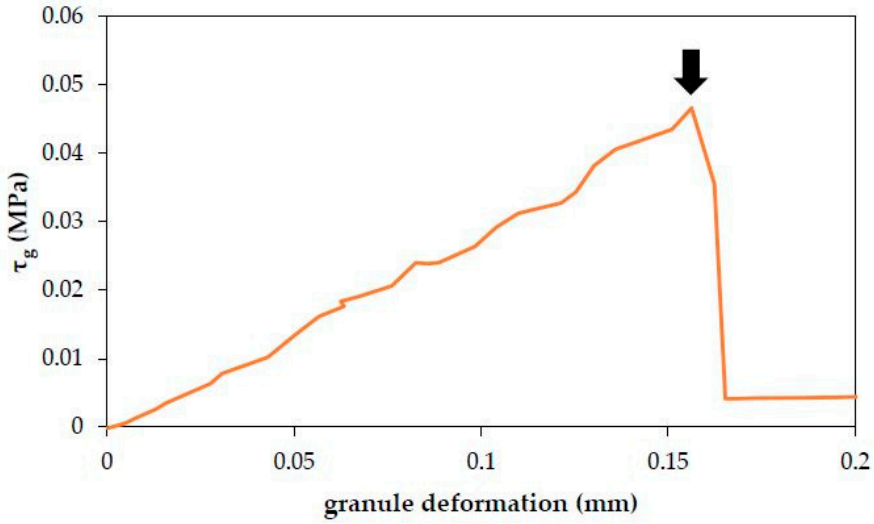


Figure 6. Typical granule stress profile versus deformation (G1, granule diameter by image analysis 3.3 mm, test temperature 74 °C).

Table 5. Average particle–binder slurry flow stress and deviation for the tested granules.

Run	X_1 (%)	X_2 (wt%)	X_3 (°C)	τ_g (MPa)	Σ (MPa)	T_{TEST} (°C)
G1	0	10	90	0.045	0.022	74
G3	0	20	90	0.035	0.015	78
G5	0	15	80	0.076	0.010	70
G8	100	15	100	0.026	0.013	70
Average				**0.045**		

Table 6 presents the measured values for each run envelope density (ρ_E), particle density (ρ_s), granules' porosity (ε) and the corresponding dimensionless numbers St_{def} and s_{max}. As it can be seen, porosities range between 0.018 and 0.216; 0.107 is the average value for all runs. In general, granules' porosity is rarely reported in the literature, which is mainly because it is a variable quite difficult to measure considering that it must consider the pores that are formed between the particles and binder during the granulation process. In this case, lower porosities than those reported by Walker et al. [9] are found, although these authors used an average porosity of 0.17 for s_{max} calculation and stated that it was independent of the mass of binder. In our case, porosity tends to decrease with temperature, while as observed by Walker, no clear trend with W_{PEG} and fluidization air velocity is found. Indeed, high temperatures favor binder spreading due to lower viscosities, filling all the internal pores within the granules. Considering that most of the obtained s_{max} are higher than 1, it is possible to infer that the process involves the formation of granules where binder can fill most of the internal voids. Regarding St_{def}, the values are within 0.0187 and 0.0726, widening the spectra of deformation values tested by Walker et al. [9], taking into account that in the present contribution, variations in fluidization air flowrate are considered.

Table 6. Measured variables and dimensionless numbers for al runs.

Run	ρ_E (g/mL)	ρ_S (g/mL)	ε (-)	s_{max} (-)	St_{def} (-)
G1	1.28	1.48	0.134	1.24	0.0583
G2	1.24	1.48	0.162	0.99	0.0187
G3	1.16	1.44	0.196	1.76	0.0565
G4	1.28	1.44	0.111	3.45	0.0195
G5	1.30	1.46	0.107	2.53	0.0625
G6	1.17	1.46	0.199	1.22	0.0187
G7	1.43	1.46	0.018	16.77	0.0726
G8	1.37	1.46	0.060	4.72	0.0216
G9	1.35	1.48	0.086	2.04	0.0356
G10	1.13	1.44	0.216	1.56	0.0298
G11	1.42	1.48	0.037	5.02	0.0444
G12	1.32	1.44	0.086	4.57	0.0279
G13	1.36	1.46	0.070	4.00	0.0346
G14	1.37	1.46	0.064	4.45	0.0395
G15	1.38	1.46	0.057	5.02	0.0420

Overall, Figure 7 depicts the obtained dimensionless numbers on the regime map proposed by Iveson and Litster [22,23] and later extended to predict granules' growth in FBMG by Walker´s group [9,24]. G7 was excluded from the map to better visualize the runs' spread. As it can be seen, most of the runs fall within the rapid growth area. That is, final granules are formed by the agglomeration of multiple smaller granules, giving a broad PSD that is substantially bigger than the initial seeds. Indeed, this is indicated by the values of mean diameters reported in Table 2, which are one order of magnitude bigger than that corresponding to lactose (d_{50} = 0.038 mm). As an example, the SEM images of selected representative runs (G1 and G5) are shown in Figure 8. As it can be seen, as the pore saturation increases (i.e., greater than 1), granules are formed by the agglomeration of smaller granules (G1). Furthermore, when the binder content is high and it is able to wet the external surface, small lactose particles adhere to the granules, promoting a growth similar to coating. Similar results were observed by Korteby et al. [6], who observed that a large binder particle size, such as the one used in this study, together with high binder viscosity (G5 presents low T_A) promotes the successful attachment of filler particles to the surface of the binder. The runs that present higher fluidization air flowrates (red symbols) are within high deformation numbers. As the collision velocity between granules increases, it is expected to favor granules' deformation. The opposite occurs for the lower fluidization air flowrates (gray symbols). Still, fluidization air velocities are low enough to avoid a crumb type of growth. In fact, all granules seem well consolidated, suggesting that breakage is not the dominating process. Regarding T_A, it is possible to observe that at higher fluidization air temperature, there is higher pore saturation (i.e., solid symbols −80 °C are toward the left of the map while stripped −90 °C and empty −100 °C are more to the right), meaning that the melted binder can fill and saturate the granules' pores. As previously explained, this can be related to the decrease in viscosity at higher temperatures. Finally, for W_{PEG}, even if squares (20 wt%), circles (15 wt%), and triangles (10 wt%) are found across the regime map, there is a greater concentration of intermediate and high binder mass content toward the right, indicating that more PEG in the system favors the formation of granules with saturated pores.

Regarding growth regimes, most of the runs are categorized as rapid growth, there are two runs with steady growth (G1 and G6) and one in the nucleation area (G2). Particularly, these three runs present the worst flowability (Table 2 and Figure 3), indicating that the combination of operating variables hinders the production of big granules with smooth surfaces.

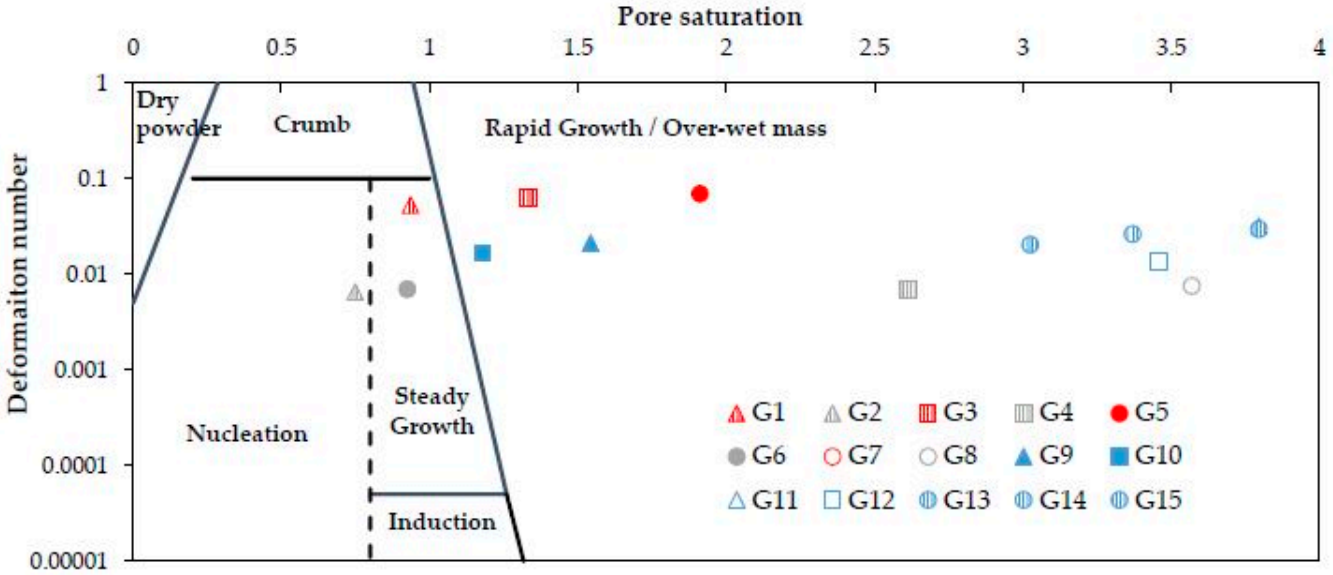


Figure 7. Walker's regime map with obtained experimental points. Symbols for W_{PEG}: square: 20 wt%, circle: 15 wt%, triangle: 10 wt%. Colors for bypass valve aperture: red: 0%, blue: 50%, gray: 100%. Infill for T_A: solid: 80 °C, striped: 90 °C, empty: 100 °C.

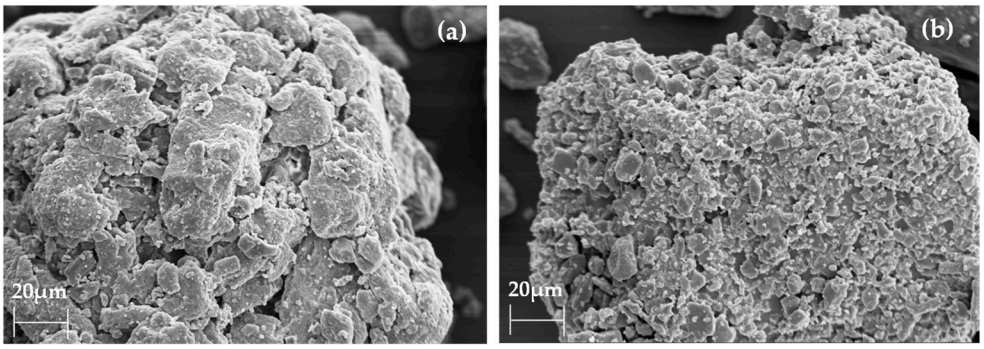


Figure 8. SEM Images of selected granules. (**a**) Run G1 granule x1500. (**b**) Run G5 granule x1500.

4. Conclusions

There is a great interest in understanding the granule growth mechanisms and the effects of process conditions over granules' quality and the operation efficiency for the co-melt fluidized bed granulation. In this sense, this work studies, by a Box–Behnken approach, the combined effect of binder mass content and fluidization air flow rate and temperature on granules' quality (particle size distribution, morphology, flow properties) and process-related variables (mass of granules collected as product in the granulator chamber, fines elutriation, and loss due to wall stickiness). It was found that binder content has a direct effect on the granules' size, and its increment also improves powder flowability. Furthermore, more granules are collected as product within the granulator for higher binder content. Regarding fluidization air temperature, it affects binder viscosity, impacting on the particle–particle liquid bridges' strength. Interestingly, for medium and coarse-size granules, higher temperatures tend to decrease their size. Furthermore, high air temperatures significantly enhance the process efficiency, since more granules are collected as product. Regarding the fluidization air flowrate, it affects the amount of particles smaller than d_{10} in the system, promoting the formation of small particles due to breakage at high flowrate values as well as the presence of non-elutriated powder at low flowrates. Consequently, intermediate air flowrates are optimal for obtaining more mass collected as product. Regarding regime map studies, most runs were located in the rapid growth regime, according to the high pore saturation of the obtained granules. This result agrees

with the high increment in particle size observed with respect to the initial seeds and the morphology of the final granules. Therefore, it was possible to extend Walker´s regime map, identifying the growth regimes for runs that incorporate variations in fluidization air flowrate and temperature.

Author Contributions: Conceptualization, I.M.C. and J.P.; methodology, J.C.L.d.P.; software, J.C.L.d.P.; formal analysis, J.C.L.d.P., I.M.C. and J.P.; investigation, J.C.L.d.P., I.M.C. and J.P.; writing—original draft preparation, J.C.L.d.P.; writing—review and editing, I.M.C. and J.P.; supervision, I.M.C. and J.P.; project administration, I.M.C. and J.P.; funding acquisition, I.M.C. and J.P. All authors have read and agreed to the published version of the manuscript.

Funding: This research was funded by the Consejo Nacional de Investigaciones Científicas y Técnicas (CONICET) through PIP 11220200102762CO, Agencia Nacional de Promoción Científica y Tecnológica (ANPCyT) through PICT-2021-CAT-I00116 and Universidad Nacional del Sur (UNS) of Argentina through PGI 24M/163.

Institutional Review Board Statement: Not applicable.

Informed Consent Statement: Not applicable.

Data Availability Statement: Data are contained within the article.

Acknowledgments: The authors also express their gratitude to DFE PHARMA through Chutrau Argentina for gently donating the lactose HMS (NZ) for the experimental assays.

Conflicts of Interest: The authors declare no conflict of interest.

Appendix A

This appendix includes the equations obtained from the surface responses for d_{10} (A1), d_{50} (A2), d_{90} (A3), AR (A4), M_P (A5), M_f (A6), and M_w (A7). All the coefficients of the following equations were presented in Tables 3 and 4. In terms of the coded factors, the responses are given by the following:

$$d_{10}(mm) = 0.23 + 0.02 \times X_1 + 0.0487 \times X_2 + 0.0637 \times X_3 + 0.045 \times X_1X_2 - 0.0854 \times {X_1}^2 - 0.0579 \times {X_2}^2 - 0.0329 \times {X_3}^2 \quad \text{(A1)}$$

$$d_{50}(mm) = 0.45 - 0.0962 \times X_1 + 0.23 \times X_2 - 0.2412 \times X_3 + 0.1675 \times X_1X_3 - 0.22 \times X_2X_3 - 0.1561 \times {X_1}^2 + 0.2513 \times {X_2}^2 \quad \text{(A2)}$$

$$d_{90}(mm) = 0.55 - 0.1212 \times X_1 + 0.265 \times X_2 - 0.1837 \times X_3 + 0.2875 \times X_1X_3 + 0.4340 \times {X_2}^2 + 0.2015 \times {X_3}^2 \quad \text{(A3)}$$

$$AR = 16.87 - 3.660 \times X_2 - 3.394 \times X_1X_2 + 4.231 \times {X_1}^2 - 3.599 \times {X_3}^2 \quad \text{(A4)}$$

$$M_p(g) = 133.45 + 3.6 \times X_1 + 0.59 \times X_2 + 12.6 \times X_3 - 4 \times X_1X_2 + 7.06 \times X_1X_3 + 7.09 \times X_2X_3 - 6.06 \times {X_1}^2 - 11.51 \times {X_3}^2 \quad \text{(A5)}$$

$$M_f(g) = 5.15 + 0.37 \times X_1 + 2.75 \times X_2 - 11.63 \times X_3 - 4.25 \times X_1X_3 - 7 \times X_2X_3 + 3.48 \times {X_1}^2 + 8.98 \times {X_3}^2 \quad \text{(A6)}$$

$$M_W(g) = 3.23 - 1.29 \times X_1 - 1.89 \times X_2 - 2.23 \times X_3 + 1.73 \times {X_2}^2 + 1.57 \times {X_3}^2 \quad \text{(A7)}$$

References

1. Meng, W.; Rao, K.S.; Snee, R.D.; Ramachandran, R.; Muzzio, F.J. A comprehensive analysis and optimization of continuous twin-screw granulation processes via sequential experimentation strategy. *Int. J. Pharm.* **2019**, *556*, 349–362. [CrossRef] [PubMed]
2. Barrasso, D.; Ramachandran, R. Multi-scale modeling of granulation processes: Bi-directional coupling of PBM with DEM via collision frequencies. *Chem. Eng. Res. Des.* **2015**, *93*, 304–317. [CrossRef]
3. Bertín, D.; Cotabarren, I.M.; Moraga, S.V.; Piña, J.; Bucalá, V. The effect of binder concentration in fluidized-bed granulation: Transition between wet and melt granulation. *Chem. Eng. Res. Des.* **2018**, *132*, 162–169. [CrossRef]
4. Moraga, S.V.; Villa, M.P.; Bertín, D.E.; Cotabarren, I.M.; Piña, J.; Pedernera, M.; Bucalá, V. Fluidized-bed melt granulation: The effect of operating variables on process performance and granule properties. *Powder Technol.* **2015**, *286*, 654–667. [CrossRef]
5. Pohl, S.; Kleinebudde, P. A review of regime maps for granulation. *Int. J. Pharm.* **2020**, *587*, 119660. [CrossRef]
6. Korteby, Y.; Kristó, K.; Sovány, T.; Regdon, G. Use of machine learning tool to elucidate and characterize the growth mechanism of an in-situ fluid bed melt granulation. *Powder Technol.* **2018**, *331*, 286–295. [CrossRef]
7. Kukec, S.; Vrečer, F.; Dreu, R. A study of in situ fluid bed melt granulation using response surface methodology. *Acta Pharm.* **2012**, *62*, 497–513. [CrossRef]
8. Walker, G.; Andrews, G.; Jones, D. Effect of process parameters on the melt granulation of pharmaceutical powders. *Powder Technol.* **2006**, *165*, 161–166. [CrossRef]
9. Walker, G.M.; Holland, C.R.; Ahmad, M.M.; Craig, D.Q. Influence of process parameters on fluidised hot-melt granulation and tablet pressing of pharmaceutical powders. *Chem. Eng. Sci.* **2005**, *60*, 3867–3877. [CrossRef]
10. Walker, G.; Bell, S.; Andrews, G.; Jones, D. Co-melt fluidised bed granulation of pharmaceutical powders: Improvements in drug bioavailability. *Chem. Eng. Sci.* **2007**, *62*, 451–462. [CrossRef]
11. Zhai, H.; Li, S.; Jones, D.; Walker, G.; Andrews, G. The effect of the binder size and viscosity on agglomerate growth in fluidised hot melt granulation. *Chem. Eng. J.* **2010**, *164*, 275–284. [CrossRef]
12. Zhai, H.; Li, S.; Andrews, G.; Jones, D.; Bell, S.; Walker, G. Nucleation and growth in fluidised hot melt granulation. *Powder Technol.* **2009**, *189*, 230–237. [CrossRef]
13. Mangwandi, C.; Zainal, N.; JiangTao, L.; Glocheux, Y.; Albadarin, A.B. Investigation of influence of process variables on mechanical strength, size and homogeneity of pharmaceutical granules produced by fluidised hot melt granulation. *Powder Technol.* **2015**, *272*, 173–180. [CrossRef]
14. Ansari, M.A.; Stepanek, F. Formation of hollow core granules by fluid bed in situ melt granulation: Modelling and experiments. *Int. J. Pharm.* **2006**, *321*, 108–116. [CrossRef] [PubMed]
15. Kidokoro, M.; Haramiishi, Y.; Sagasaki, S.; Shimizu, T.; Yamamoto, Y. Application of fluidized hot-melt granulation (fhmg) for the preparation of granules for tableting; properties of granules and tablets prepared by fhmg. *Drug Dev. Ind. Pharm.* **2002**, *28*, 67–76. [CrossRef]
16. Passerini, N.; Calogerà, G.; Albertini, B.; Rodriguez, L. Melt granulation of pharmaceutical powders: A comparison of high-shear mixer and fluidised bed processes. *Int. J. Pharm.* **2010**, *391*, 177–186. [CrossRef]
17. Prado, H.J.; Bonelli, P.R.; Cukierman, A.L. In situ fluidized hot melt granulation using a novel meltable binder: Effect of formulation variables on granule characteristics and controlled release tablets. *Powder Technol.* **2014**, *264*, 498–506. [CrossRef]
18. Pauli-Bruns, A.; Knop, K.; Lippold, B.C. Preparation of sustained release matrix pellets by melt agglomeration in the fluidized bed: Influence of formulation variables and modelling of agglomerate growth. *Eur. J. Pharm. Biopharm.* **2010**, *74*, 503–512. [CrossRef]
19. Mašić, I.; Ilić, I.; Dreu, R.; Ibrić, S.; Parojčić, J.; Đurić, Z. An investigation into the effect of formulation variables and process parameters on characteristics of granules obtained by in situ fluidized hot melt granulation. *Int. J. Pharm.* **2012**, *423*, 202–212. [CrossRef]
20. Mašić, I.; Ilić, I.; Dreu, R.; Ibrić, S.; Parojčić, J.; Srčič, S. Melt granulation in fluidized bed: A comparative study of spray-on versus*in situ*procedure. *Drug Dev. Ind. Pharm.* **2014**, *40*, 23–32. [CrossRef]
21. Aleksić, I.; Đuriš, J.; Ilić, I.; Ibrić, S.; Parojčić, J.; Srčič, S. In silico modeling of in situ fluidized bed melt granulation. *Int. J. Pharm.* **2014**, *466*, 21–30. [CrossRef] [PubMed]
22. Iveson, S.M.; Litster, J.D. Growth regime map for liquid-bound granules. *AIChE J.* **1998**, *44*, 1510–1518. [CrossRef]
23. Iveson, S.M.; Wauters, P.A.; Forrest, S.; Litster, J.D.; Meesters, G.M.; Scarlett, B. Growth regime map for liquid-bound granules: Further development and experimental validation. *Powder Technol.* **2001**, *117*, 83–97. [CrossRef]
24. Walker, G.; Bell, S.; Vann, M.; Zhai, H.; Jones, D.; Andrews, G. Pharmaceutically Engineering Powders Using FHMG: The effects of process parameters and formulation variables. *Chem. Eng. Res. Des.* **2007**, *85*, 981–986. [CrossRef]
25. Desai, U.S.; Chaudhari, P.; Bhavsar, D.B.; Chavan, R.P. Melt granulation: An alternative to traditional granulation techniques. *Indian Drugs* **2013**, *50*, 5–13. [CrossRef]
26. Montgomery, D.C. *Design and Analysis of Experiments*; Wiley & Sons: New York, NY, USA, 2005.
27. Rattes, A.L.R.; Oliveira, W.P. Spray drying conditions and encapsulating composition effects on formulation and properties of sodium diclofenac microparticles. *Powder Technol.* **2007**, *171*, 7–14. [CrossRef]
28. Schüssele, A.; Bauer-Brandl, A. Note on the measurement of flowability according to the European Pharmacopoeia. *Int. J. Pharm.* **2003**, *257*, 301–304. [CrossRef]

29. *United States Pharmacopeia and National Formulary*; USP 30-NF; United States Pharmacopeial Conv.: Rockville, MD, USA, 2007.
30. Abberger, T.; Seo, A.; Schæfer, T. The effect of droplet size and powder particle size on the mechanisms of nucleation and growth in fluid bed melt agglomeration. *Int. J. Pharm.* **2002**, *249*, 185–197. [CrossRef]

Disclaimer/Publisher's Note: The statements, opinions and data contained in all publications are solely those of the individual author(s) and contributor(s) and not of MDPI and/or the editor(s). MDPI and/or the editor(s) disclaim responsibility for any injury to people or property resulting from any ideas, methods, instructions or products referred to in the content.